Developmental Cell
Article

AGO4 Regulates Entry into Meiosis and Influences Silencing of Sex Chromosomes in the Male Mouse Germline

Andrew J. Modzelewski,[1,3] Rebecca J. Holmes,[1,3,4] Stephanie Hilz,[2] Andrew Grimson,[2,*] and Paula E. Cohen[1,*]
[1]Department of Biomedical Sciences, College of Veterinary Medicine
[2]Department of Molecular Biology and Genetics, College of Arts and Sciences
Cornell University, Ithaca, NY 14853, USA
[3]These authors contributed equally to this work
[4]Present address: Boston IVF, The Waltham Center, 130 Second Avenue, Waltham, MA 02451, USA
*Correspondence: agrimson@cornell.edu (A.G.), paula.cohen@cornell.edu (P.E.C.)
http://dx.doi.org/10.1016/j.devcel.2012.07.003

SUMMARY

The four mammalian Argonaute family members are thought to share redundant functions in the microRNA pathway, yet only AGO2 possesses the catalytic "slicer" function required for RNAi. Whether AGO1, AGO3, or AGO4 possesses specialized functions remains unclear. Here we show that AGO4 localizes to spermatocyte nuclei during meiotic prophase I, specifically at sites of asynapsis and the transcriptionally silenced XY subdomain, the sex body. We generated *Ago4* knockout mice and show that *Ago4*$^{-/-}$ spermatogonia initiate meiosis early, resulting from premature induction of retinoic acid-response genes. During prophase I, the sex body assembles incorrectly in *Ago4*$^{-/-}$ mice, leading to disrupted meiotic sex chromosome inactivation (MSCI). This is associated with a dramatic loss of microRNAs, >20% of which arises from the X chromosome. Thus, AGO4 regulates meiotic entry and MSCI in mammalian germ cells, implicating small RNA pathways in these processes.

INTRODUCTION

Argonaute proteins form two clades within a larger superfamily, based on their sequence homology (Cenik and Zamore, 2011; Czech and Hannon, 2011). The PIWI clade includes *Mili*, *Miwi1*, and *Miwi2* in mice, which are required for retrotransposon silencing in the germline and normal progression through prophase I in male meiosis (Aravin et al., 2006; Girard et al., 2006; Grivna et al., 2006), in conjunction with the PIWI-interacting RNAs (piRNAs). The second clade is comprised of the AGO proteins, of which there are four in mammals (AGO1–AGO4; Steiner and Plasterk, 2006). However, only AGO2 is capable of mediating small RNA-directed endonucleolytic cleavage of mRNA targets, the hallmark of RNAi (Liu et al., 2004; Meister et al., 2004; Song et al., 2003). No individual functions have yet been ascribed to the other mammalian AGOs, but they can all associate with several distinct classes of small RNAs, including microRNAs (miRNAs) and small interfering RNAs (siRNAs).

Endogenous siRNAs and miRNAs are found in the male germline (Song et al., 2011; Watanabe et al., 2006), and whereas some associate with AGO proteins (Kim et al., 2006), their precise roles are unknown. Small RNAs may function in the process of meiotic silencing of unpaired chromosomes, a common feature of prophase I in a number of organisms (Maine, 2010). During meiosis in *Neurospora crassa*, for example, the presence of unsynapsed DNA triggers the posttranscriptional silencing of any homologous sequences. This process, called meiotic silencing of unpaired DNA (MSUD), requires Ago protein function and small RNA involvement (Raju et al., 2007; Shiu et al., 2001).

The high expression of mouse *Ago4* (and *Ago3)* in the male germline (González-González et al., 2008) indicates that similar meiotic functions for AGO proteins may also exist in mammals. Two distinct levels of meiotic silencing in the male germline have been described: meiotic silencing of unsynapsed chromatin (MSUC; Schimenti, 2005) and meiotic sex chromosome inactivation (MSCI; Fernandez-Capetillo et al., 2003; Turner, 2007). MSUC monitors complete pairing before permitting progression through prophase I and protects the genome from transposon mobilization by silencing regions that fail to pair because of hemizygous transposon insertions (Turner et al., 2005). MSCI, on the other hand, is unique to the sex chromosomes and results in their heterochromatinization and compartmentalization into a specialized nuclear subdomain known as the sex body (SB; Handel, 2004). This enables the unpaired sex chromatin to bypass meiotic synapsis check points and is essential for meiotic progression in males (Baarends and Grootegoed, 2003). Although neither mechanism is fully understood, it is notable that the miRNA genes located on the X chromosome evade MSCI, perhaps indicating a role for small RNAs in silencing (Song et al., 2009).

To examine the role of AGO4 in mammals, we generated an *Ago4* null mouse line. *Ago4*$^{-/-}$ mice are viable, but males have fertility defects including reduced testis size and lower sperm counts. AGO4 localizes to the SB during pachynema of prophase I, and loss of *Ago4* perturbs SB morphology leading to an influx of RNA polymerase II (RNAP II), and an associated failure to silence many sex-linked transcripts, resulting in

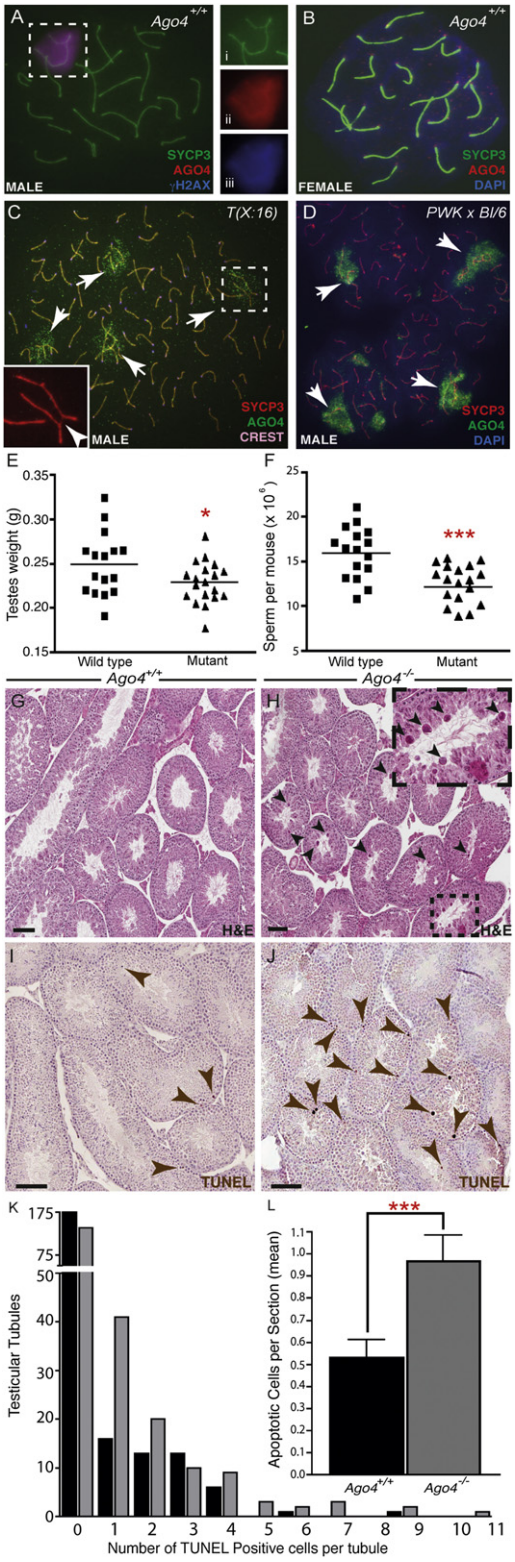

Figure 1. AGO4 Localization and Phenotypic Analysis of *Ago4*$^{-/-}$ Males

(A–D) AGO4 localization on chromosome spreads from wild-type (WT) and induced asynaptic mouse models. (A) Spermatocyte from a WT mouse stained with anti-SYCP3 (i, green), anti-AGO4 (ii, red), and anti-γH2AX (iii, blue). (B) Pachytene stage oocyte from WT mouse stained with anti-SYCP3 (green) and anti-AGO4 (red) antibodies and DAPI to highlight DNA (blue). (C and D) Pachytene stage spermatocytes from a T(X:16) male translocation mouse (C) and a PWK × C57BL/6J hybrid mouse (D) that both exhibit significant levels of asynapsis (arrows), stained with anti-SYCP3 (red), CREST autoimmune serum (pink localization on centromeres in C only), and anti-AGO4 (green) antibodies. Asynapsis induced by chromosome 16 to X translocation in (C) is marked by white arrowhead (inset). Dashed-line boxes in (A) and (C) identify the region that is further magnified in the corresponding inset panels.

(E) Testes from *Ago4*$^{-/-}$ mice (n = 19) are significantly reduced in size compared to WT (n = 16; *$p < 0.05$, t test).

(F) Caudal epididymal sperm counts shown in millions. Sperm counts from *Ago4*$^{-/-}$ mice (▲ n = 19) are reduced when compared to WT (■ n = 16; ***$p < 0.0005$, t test).

(G and H) Testis sections from (G) *Ago4*$^{+/+}$ and (H) *Ago4*$^{-/-}$ mice with H&E. Scale bars, 100 μm. Large multinucleated cells are apparent in *Ago4*$^{-/-}$ mice (arrowheads and inset).

(I and J) TUNEL staining and quantitation of testis sections from (I) *Ago4*$^{+/+}$ and (J) *Ago4*$^{-/-}$ mice.

(K and L) *Ago4*$^{+/+}$ (black bars) and *Ago4*$^{-/-}$ mice (gray bars) expressed per tubule (K) or per section (L) showing significant increase in *Ago4*$^{-/-}$ mice (n = 230, 45.2% increase; ***$p < 0.0005$, t test). Error bars, SEM.

See Figure S1 and Table S1.

apoptosis. Interestingly, our analysis also reveals an unexpected role for AGO4 in the onset of meiosis, in that spermatogonia from *Ago4*$^{-/-}$ males enter prophase I prematurely. These findings reveal a role for nonslicing Argonautes in mammalian germ cell development.

RESULTS AND DISCUSSION

AGO4 Localizes to the Sex Body during Prophase I of Meiosis

In adult mouse testis, *Ago4* mRNA expression is highest at prophase I during pachynema (González-González et al., 2008), the stage at which homologous autosomes are completely synapsed (paired), and the SB is formed. AGO4 protein localization was assessed on chromosome-spread preparations from prophase I spermatocytes of wild-type (WT) adult male testes (day 70 postpartum [pp]), together with staining of the synaptonemal complex (SC) using antibodies against the lateral element protein, SYCP3 (Figure 1A). AGO4 staining was evident in the nucleus, with the most intense staining at the SB (Figure 1Aii), where it colocalizes with γH2AX (Figure 1Aiii). The AGO4 SB staining pattern was lost when the antibody was preincubated with the immunizing peptide, indicating specificity of the signal for AGO4 (see Figure S1A available online), and no AGO4 staining was observed from *Ago4*-deficient males (Figures S1B and S1C). Only faint punctate staining was observed in oocytes (Figure 1B), which do not possess an SB.

To explore whether the meiotic localization of AGO4 to the X and Y chromosomes is a consequence of their lack of pairing, we examined the localization of AGO4 in two mouse models displaying varying degrees of induced autosomal asynapsis in spermatocytes: mice carrying a T(X:16)16H translocation (Figure 1C), or hybrid offspring of two divergent strains (PWKxB6, Figure 1D). In both cases, significant degrees of autosomal asynapsis were evident by the staining pattern for SYCP3 (Figure 1C, arrowhead), and AGO4 colocalized to all these sites (Figures 1C and 1D, arrows). Given that these asynapsed regions of

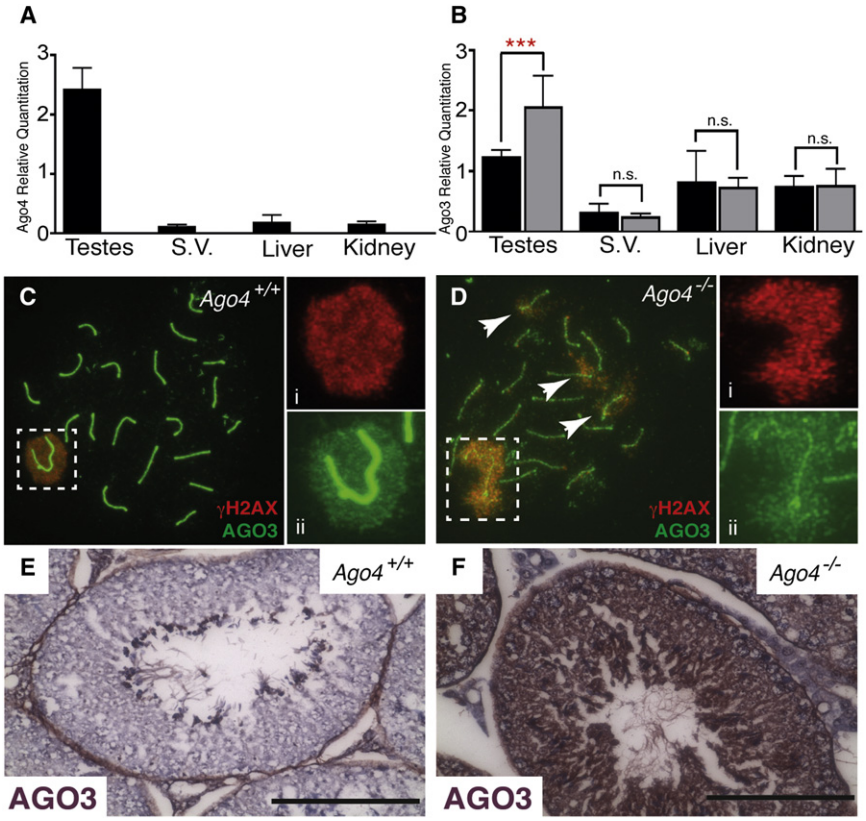

Figure 2. Upregulation of *Ago3* mRNA and Protein in the Testis of *Ago4*$^{-/-}$ Males

(A and B) Quantitative RT-PCR analysis of *Ago4* (A) and *Ago3* (B) expression in total RNA from whole testes, seminal vesicle (S.V.), liver, and kidney isolated from *Ago4*$^{+/+}$ (n = 5, black bars) and *Ago4*$^{-/-}$ (n = 5, gray bars) adult littermates (***$p < 0.001$, t test). Error bars, SEM. n.s., not significant.

(C and D) Spermatocyte spreads from *Ago4*$^{+/+}$ (C) and *Ago4*$^{-/-}$ (D) males stained with anti-γH2AX (red, Ci and Di) and anti-AGO3 (green, Cii and Dii) antibodies and DAPI (blue). "Pseudosex body" regions in (D) denoted by arrows. Dashed-line boxes identify the region that is further magnified in the corresponding inset panels. In both cases these boxes define the SB.

(E and F) Testis sections from *Ago4*$^{+/+}$ (E) and *Ago4*$^{-/-}$ (F) stained with anti-AGO3 antibody to demonstrate increased AGO3 signal within germ cells of *Ago4*$^{-/-}$ males.

See also Figure S2.

chromatin are silenced during prophase I (Handel, 2004), these observations suggest a role for AGO4 in meiotic silencing.

Loss of Ago4 Results in Reduced Testis Size and Epididymal Spermatozoa Together with Increased Apoptosis of Spermatogenic Cells

We generated a floxed *Ago4*$^{-/-}$ mouse line that, following Cre-driven excision of a *LoxP*-flanked region, lacks exons 3–17 of the gene (Figure S1D; Supplemental Experimental Procedures). The recombinant allele was backcrossed for six generations from the mixed 129/C57 background onto a pure C57Bl/6J background. Backcrossed homozygous *Ago4*$^{-/-}$ male and female mice were healthy and viable, and male and female offspring were observed at the expected frequencies (male, 54%; female, 46%; n = 121). Furthermore, *Ago4*$^{-/-}$ males exhibit normal mating behavior with no decrease in litter sizes from *Ago4*$^{+/+}$ males (Table S1). However, testis weights in *Ago4*$^{-/-}$ adult mice were reduced by 13% compared to *Ago4*$^{+/+}$ mice (Figure 1E; Table S1). Similarly, epididymal spermatozoa counts were also abnormal in *Ago4*$^{-/-}$ mice, reduced by 22% compared to WT littermates (Figure 1F; Table S1).

Testes from *Ago4*$^{-/-}$ Males Undergo Increased Apoptosis

Histological analysis with H&E revealed similar cellular composition of the seminiferous epithelium in *Ago4*$^{+/+}$ and *Ago4*$^{-/-}$ males (Figures 1G and 1H). In the latter, however, we observed abnormally large, densely staining cells within the seminiferous tubular lumen (Figure 1H). TUNEL staining of testis sections (Figures 1I and 1J) revealed a significant increase in apoptotic cells within the prophase I layers of the seminiferous epithelium of *Ago4*$^{-/-}$ mice compared to WT (Figures 1I and 1J, arrowheads; Figures 1K and 1L). These results demonstrate that *Ago4*$^{-/-}$ mice exhibit an increase in testicular apoptosis, reduced testes weight, and lowered sperm counts, phenotypes previously observed in MSCI-compromised animals (Turner et al., 2004).

Loss of AGO4 Results in Increased AGO3 Protein

Given the high degree of sequence similarity (Cenik and Zamore, 2011), together with the high expression of *Ago3* in testis, we reasoned that overlapping functions might exist between mammalian Argonaute genes. Therefore, we used quantitative reverse-transcription PCR to measure the expression of all four AGO family members in testes of *Ago4*$^{+/+}$ and *Ago4*$^{-/-}$ mice. As expected, both *Ago3* and *Ago4* mRNA are highly expressed in adult testes, and at higher levels than in all other tissues examined (Figures 2A and 2B). *Ago1* was expressed at lower and more uniform levels throughout all of the tissues, and *Ago2* expression was higher in nonmeiotic tissues (Figure S2). Loss of *Ago4* resulted in a significant increase in *Ago3* expression specifically in testis (Figure 2B; $p < 0.05$, t test), whereas *Ago1* and *Ago2* transcripts were not affected by the loss of AGO4 (Figure S2). Together, these data suggest that *Ago3* and *Ago4* may function redundantly in the male germline, such that loss of *Ago4* results in a compensatory elevation in *Ago3* mRNA.

We next investigated whether AGO3 protein shows similar localization to AGO4 on male prophase I chromosome spreads. Like AGO4, AGO3 localized preferentially to the SB at pachynema in WT spreads (Figure 2Ci). When examining the AGO3 staining pattern on *Ago4*$^{-/-}$ spreads, however, we found that the chromatin domain occupied by AGO3 signal was dramatically expanded (Figure 2D). Indeed, both AGO3 and γH2AX extended beyond the SB into areas of chromatin associated

with the autosomes (Figure 2D, arrows). In mouse mutants that exhibit similar disruption of the SB appearance, these extended γH2AX domains have been termed "pseudosex bodies" (Barchi et al., 2005; Bellani et al., 2005; Daniel et al., 2011).

AGO3 localization was also assessed by immunohistochemistry of whole testis sections from *Ago4*$^{+/+}$ and *Ago4*$^{-/-}$ adult males. In WT testis, AGO3 localized to meiotic cells and was absent in the nonmeiotic spermatogonial cells (Figure 2E). In *Ago4*$^{-/-}$ testis, AGO3 signal was increased (Figure 2F), as expected, but still restricted to spermatogenic cells. Thus, the loss of *Ago4* results in increased expression of *Ago3* in the testis. We conclude that some functions of AGO4 in the male germline may be redundant with AGO3, and, if so, this would imply that the testis weight and sperm count phenotypes observed in *Ago4*$^{-/-}$ mice result from only a partial defect in these shared functions.

Loss of AGO4 Disrupts SB Formation and Alters the Localization of Key SB Components

To examine more closely the SB morphology of *Ago4*$^{-/-}$ males, we investigated the localization of the SC central element protein, SYCP1, together with SYCP3 during prophase I (Figure 3A). In *Ago4*$^{-/-}$ spreads, SYCP1 localized to unsynapsed regions of the X and Y (Figure 3B) approximately 4-fold more frequently than in the WT (Figure 3C; *Ago4*$^{+/+}$ 6.3%, *Ago4*$^{-/-}$ 22.8% of 300 pachytene spermatocytes; $p < 0.0005$, χ^2 test), indicating that loss of AGO4 perturbs SC formation and/or integrity within the SB. Importantly, initial events of prophase I progression, including the processing of double-strand breaks (DSBs) for recombination, and crossover formation, appeared normal in *Ago4*$^{-/-}$ males (data not shown).

The mislocalization of SC components in the *Ago4*$^{-/-}$ SB, together with the importance of SB integrity for MSCI, led us to hypothesize that AGO4 may play a role in transcriptional silencing of the X and Y chromosomes. To test this, we utilized a repertoire of antibodies (γH2AX, TOPBP1, ATR, pCHK2, SUMO1, UbiH2A) against SB components to assess the integrity and functionality of this structure. The histone variant H2AX (histone 2A family member X) is phosphorylated during prophase I by the ATM and ATR kinases to become γH2AX (Turner et al., 2004). SB-associated H2AX phosphorylation is mediated by ATR during pachynema, a stage at which γH2AX is found almost exclusively in the SB and at any remaining asynapsed regions on autosomes (Figure 3D). However, a large proportion of *Ago4*$^{-/-}$ pachytene cells (Figures 3E and 3F, 31% versus 5.5% in WT; n = 300; $p < 0.0005$, χ^2 test) exhibit expanded γH2AX staining beyond the SB, often associating with synapsed autosomes, or pseudosex bodies. The localization of γH2AX during diplonema is unaffected by loss of AGO4 (data not shown), and in fact such defects appear to be restricted to early pachytene spermatocytes. To illustrate this, we used an antibody against the testis-specific histone variant H1T, which localizes to chromatin from late pachynema (Lin et al., 2000). We found no instances in which the altered pseudo-SB staining of γH2AX, or other SB markers, coincided with the appearance of H1T in late pachytene or diplotene cell populations (*Ago4*$^{+/+}$ n = 289, *Ago4*$^{-/-}$ n = 241; Figures S3K–S3M). Together, these results suggest that the SB morphology defects occur in early pachynema in *Ago4*$^{-/-}$ mice. Defective *Ago4*$^{-/-}$ spermatocytes are likely to be eliminated by the pachytene checkpoint, as evidenced by the increased TUNEL staining.

One explanation for aberrant γH2AX localization in *Ago4*$^{-/-}$ mice is failure to recruit ATR, which we investigated by staining for both ATR and TOPBP1, a regulator of ATR (Kumagai et al., 2006). In WT mice, ATR staining is pronounced on the X and Y chromosome cores and throughout the SB starting from pachynema (Figure 3G). In *Ago4*$^{-/-}$ pachytene cells, however, ATR is frequently mislocalized (Figures 3H and 3I, n = 200 cells; $p < 0.0005$, χ^2 test). A range of aberrant staining patterns were observed, including a complete loss of signal at the SB, reduced X chromosome core localization, and almost complete loss of Y chromosome core localization. TOPBP1 localization is similarly altered by the loss of *Ago4* (Figures S3A and S3B). The loss of ATR at the SB coincides with increased signal on autosome cores, potentially utilizing the limited store of ATR that would normally be required to induce MSCI.

We corroborated ATR mislocalization in *Ago4*$^{-/-}$ mice using an antibody against the phospho-(Ser/Thr)ATM/ATR substrate motif (Figure S3C) and an antibody specific to phosphorylated CHK2 (Weiss et al., 2002), a substrate of ATM/ATR (Figure S3E). In both cases, ATM/ATR substrate and pCHK2 were absent in a subset of pachytene spermatocyte spreads from *Ago4*$^{-/-}$ mice (Figures S3D and S3F).

SUMO1 and ubiH2A are proteins implicated in meiotic silencing (Brown et al., 2008; Vigodner, 2009). SUMO1 first appears in zygonema localizing to the X and Y cores (data not shown) and persists into pachynema (Figure S3G). During pachynema, the ubiH2A histone mark emerges and localizes to the SB (Figure S3I; Baarends et al., 2005). SUMO1 and ubiH2A localization is abolished in a subset of *Ago4*$^{-/-}$ cells (Figures 3H and 3J). Together, these studies reveal that a subset of spermatocytes in *Ago4*$^{-/-}$ males fails to assemble a normal SB structure, leading to the appearance of pseudosex bodies and mislocalization of key SB markers.

Ago4$^{-/-}$ Mice Fail to Correctly Silence the X and Y Chromosomes during Meiosis

The defects we observed in SB components prompted us to determine whether silencing of the sex chromosomes during meiosis was normal in the absence of AGO4. The trimethylation modification of H3K9 is associated with repressed heterochromatinized DNA. During prophase I in WT male mice, H3K9me3 is primarily restricted to autosomal centromeres and the majority of the SB (Kim et al., 2007; Tachibana et al., 2007; Figure 3J). In early pachynema, loss of *Ago4* results in diffuse H3K9me3 localization in a significant portion of cells (Figures 3K and 3L; n = 300; $p < 0.0005$, χ^2 test). These results suggest that AGO4 contributes to the establishment of chromatin marks associated with silencing, but as meiosis progresses aberrant cells are either eliminated or overcome the defect.

To further assess transcriptional activity of the sex chromosomes, we compared the localization of RNAP II in WT and *Ago4*$^{-/-}$ pachytene spermatocytes. As expected, in *Ago4*$^{+/+}$ cells, RNAP II is absent from sites of silencing and heterochromatin (Figure 3M) and is excluded from the SB through pachynema. This exclusion is no longer maintained in a significant fraction of pachytene spermatocytes from *Ago4*$^{-/-}$ males (Figures 3N and 3O; *Ago4*$^{+/+}$, 7%, and *Ago4*$^{-/-}$, 25.5%; n = 200;

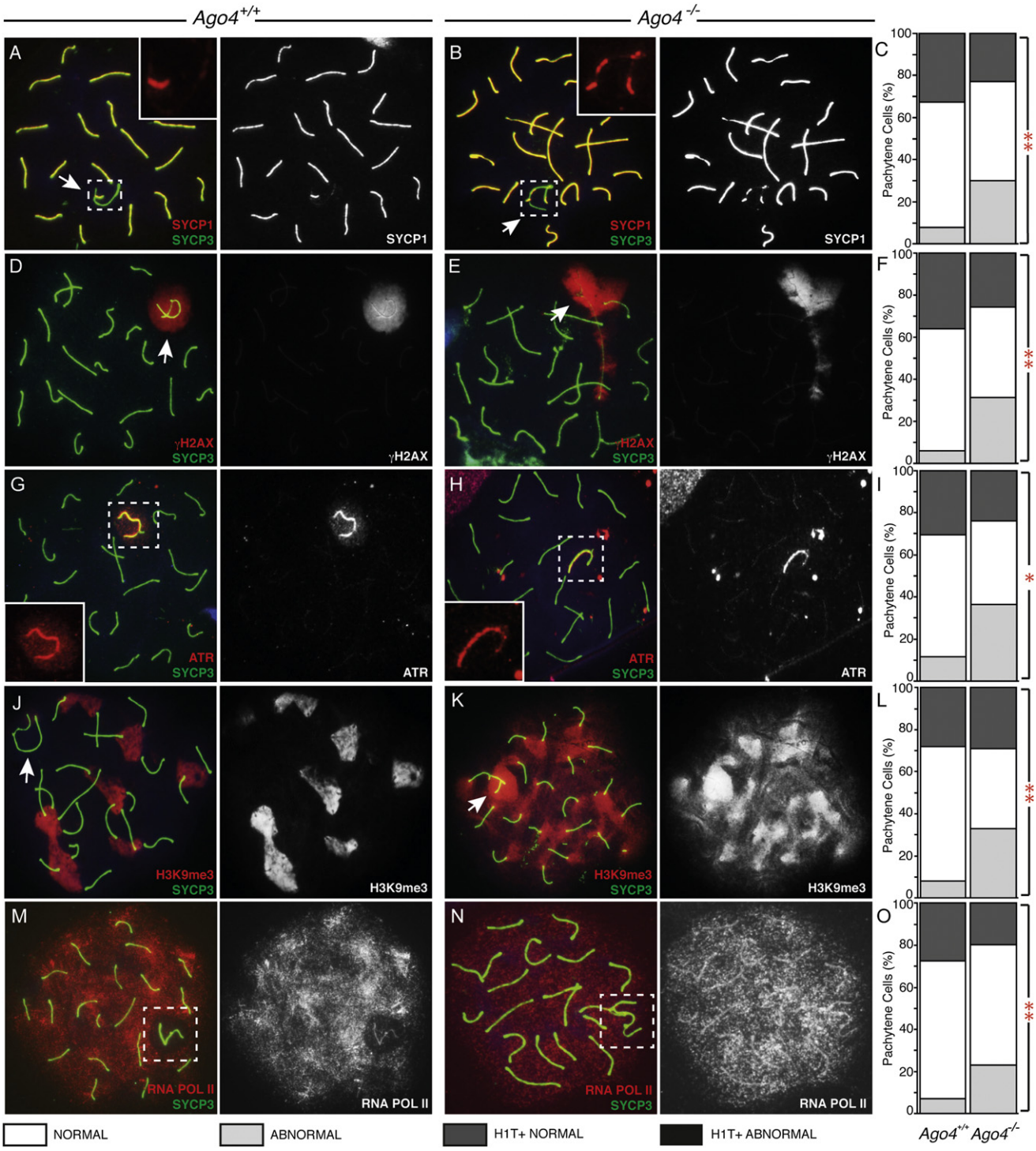

Figure 3. Loss of AGO4 Disrupts Localization of SB-Associated Proteins and RNAP II during Pachynema

Pachytene stage spermatocytes with SB (white arrows) from *Ago4*$^{+/+}$ (A, D, G, J, and M) and *Ago4*$^{-/-}$ (B, E, H, K, and N) mice, stained with anti-SYCP3 (green). For all quantitation graphs (C, F, I, L, and O), WT (left bar) and *Ago4*$^{-/-}$ (right bar).

(A–C) SYCP1 in red. Insets show magnification of SYCP1 in SB (n = 300 per genotype; **$p < 0.005$, χ^2 test).

(D–F) γH2AX in red (n = 300; **$p < 0.005$, χ^2 test).

(G–I) ATR in red (n = 200; *$p < 0.05$, χ^2 test).

(J–L) H3K9Me3 in red (n = 300; **$p < 0.005$, χ^2 test).

(M–O) RNAP II staining in red (n = 200; **$p < 0.01$, χ^2 test).

See also Figure S3.

$p < 0.0005$, χ^2 test), matching the frequency of mislocalization we observed for SB components and further indicating a silencing defect in *Ago4*$^{-/-}$ spermatocytes.

Loss of Ago4 Leads to Downregulation of Specific miRNA Families

Because Argonaute proteins function with small RNAs, we hypothesized that the phenotypes in *Ago4*$^{-/-}$ animals reflect alterations in the small RNAs. We therefore cloned and sequenced small RNAs (18–30 nt) from purified pachytene cells isolated from *Ago4*$^{+/+}$ and *Ago4*$^{-/-}$ littermates. We obtained 21.2 and 14.7 million genome-matching reads from the *Ago4*$^{+/+}$ and *Ago4*$^{-/-}$ samples, respectively, a sequencing depth sufficient to robustly profile the small RNAs of pachytene cells.

piRNAs are the most abundant small RNAs in pachytene cells (Pillai and Chuma, 2012; Siomi et al., 2011), and loss of *Ago4* only minimally perturbed these piRNA populations (Figures S4F and S4G), as expected. By contrast, loss of *Ago4* had a substantial effect on the miRNAs present in pachytene cells. Overall, we observed an approximately 2.3-fold reduction (Figures 4 and S4) in reads matching miRNA hairpins in *Ago4*$^{-/-}$ pachytene cells (Figures 4A and S4A; 6% *Ago4*$^{+/+}$, 2.6% *Ago4*$^{-/-}$). However, this reduction was not consistent among different miRNA families, indicating some degree of miRNA specificity for AGO4 (Figures 4C, 4D, S4C, S4D, and S5). Approximately 20% of the global miRNA downregulation came from miRNAs expressed from the X chromosome, and, interestingly, all miRNAs encoded on the X are significantly less abundant ($p < 0.01$, Wilcoxon rank sum test) in *Ago4*$^{-/-}$ cells, whereas not all autosomal miRNAs are decreased (Figures 4B–4E and S4B–S4E).

We considered two explanations for the alterations in the miRNA profile of *Ago4*$^{-/-}$ cells. First, AGO proteins might associate with miRNAs at different efficacies; thus, in the absence of AGO4, the sequenced miRNAs would represent the propensities of AGO1, AGO2, and AGO3 to form complexes with specific miRNAs. Second, the altered profile might be a downstream consequence of altered transcriptional regulation of miRNA genes. To distinguish between these possibilities, we compared the change in abundance for each mature miRNA sequence to each variant miRNA sequence originating from the same precursor. The normal processing of miRNA precursors (Ruby et al., 2006, 2007) results in the production of a mature miRNA species together with rarer shorter or longer variant miRNAs. Such variations can alter propensities for association with AGO proteins (Okamura et al., 2009; Wang et al., 2011), whereas alterations in the transcription of miRNA genes would be reflected equally by all variant products (isomiRs) of a particular miRNA. We found that changes in the abundance of pairs of miRNAs and variant miRNA species were significantly correlated (Figure 4F; $R = 0.68$; $p \leq 10^{-45}$; Figure S5; Table S2), a result most consistent with transcriptional differences for miRNA genes in *Ago4*$^{-/-}$ cells. Interestingly, when comparing miRs and isomiRs with shared 5′ ends and shared 3′ ends, those with shared 5′ ends were somewhat ($p = 0.09$) more correlated (Figure 4F; R values of 0.70, purple) than those with shared 3′ ends ($R = 0.41$, yellow). These results are consistent with loss of *Ago4* resulting in both changes in miRNA transcription, together with different propensities for certain miRNA species to form complexes with different AGO proteins. Importantly, loss of AGO4 results in a significant reduction in specific miRNAs, and despite increased RNAP II in the SB, a significant fraction of these arise from the X chromosome.

To correlate changes in small RNA species identified by small RNA cloning with changes in their localization, we examined the localization of miRNAs originating from the X chromosome. For example, miR-322 is known to escape MSCI (Song et al., 2009) and was shown in our small RNA cloning to be dramatically downregulated in the absence of AGO4. We find that miR-322 localizes to the SB in WT spermatocytes (Figure 4G), whereas its localization is decreased in those *Ago4*$^{-/-}$ pachytene spermatocytes that display aberrant SB morphology (Figure 4H). Furthermore, we confirm the SB localization of miR-24 as demonstrated previously (Marcon et al., 2008), and observed no signal from miR-206, consistent with the small RNA cloning data (Figures S4H and S4I). Together, these studies demonstrate that certain miRNAs are dependent on AGO4 and suggest an accumulation of some miRNA species in the SB during pachynema.

Expression Profiling of Pachytene Spermatocytes Reveals Loss of Silencing of Sex-Linked Genes

To better understand alterations in gene expression that result from loss of *Ago4*, we used RNAseq to profile the transcriptome of *Ago4*$^{-/-}$ and WT cell populations. Our profiling was performed on whole testis extracts at days 3–4 and 8–9 pp, both comprised solely of somatic cells and spermatogonia, together with isolated meiotic cell fractions from adult testis at leptonema/zygonema and at pachynema. RNA from adult kidney and seminal vesicles served as controls for each genotype.

Contrary to our expectation, we found no evidence for a global failure in sex chromosome silencing in *Ago4*$^{-/-}$ pachytene cells (Figure 5A). However, numerous Y-linked transcripts did show upregulated expression in the absence of *Ago4*, including *Zfy2* and *Ube1y1* (Figures 5B and 5C). *Zfy2* is one of the "suicide" genes (along with *Zfy1*) whose expression in the absence of MSCI results in apoptosis (Royo et al., 2010). *Zfy2* expression was elevated approximately 2-fold in pachytene spermatocytes from *Ago4*$^{-/-}$ males ($p < 0.03$). Importantly, the increased transcription seen for certain sex-linked genes in the absence of AGO4 is likely contributed only by those pachytene cells showing SB aberrations. Thus, the overall extent of the loss of silencing is likely diluted by the heterogeneous population of aberrant and normal pachytene cells obtained for RNAseq analysis. This would suggest that the effect of AGO4 loss on MSCI is underestimated by our RNAseq analysis.

Many aspects of MSCI initiation and maintenance remain elusive. Establishment of MSCI requires H2AX phosphorylation by ATR in the SB. Thus, during meiotic prophase I, ATR and γH2AX accumulate on sex chromatin in spermatocytes (Fernandez-Capetillo et al., 2003; Turner et al., 2004, 2005). The prevailing model proposes that to maintain MSCI, the limited pool of ATR functions to prevent expression of toxic Y-linked genes (Royo et al., 2010). Thus, ATR must be recruited to the SB by first being depleted from the autosomes following synapsis. In various SC or recombination repair mouse mutants, therefore, ATR persists on the autosomes due to the more generalized MSUC mechanism, resulting in upregulation of gene expression from the sex chromosomes including *Zfy1*/*Zfy2*. It

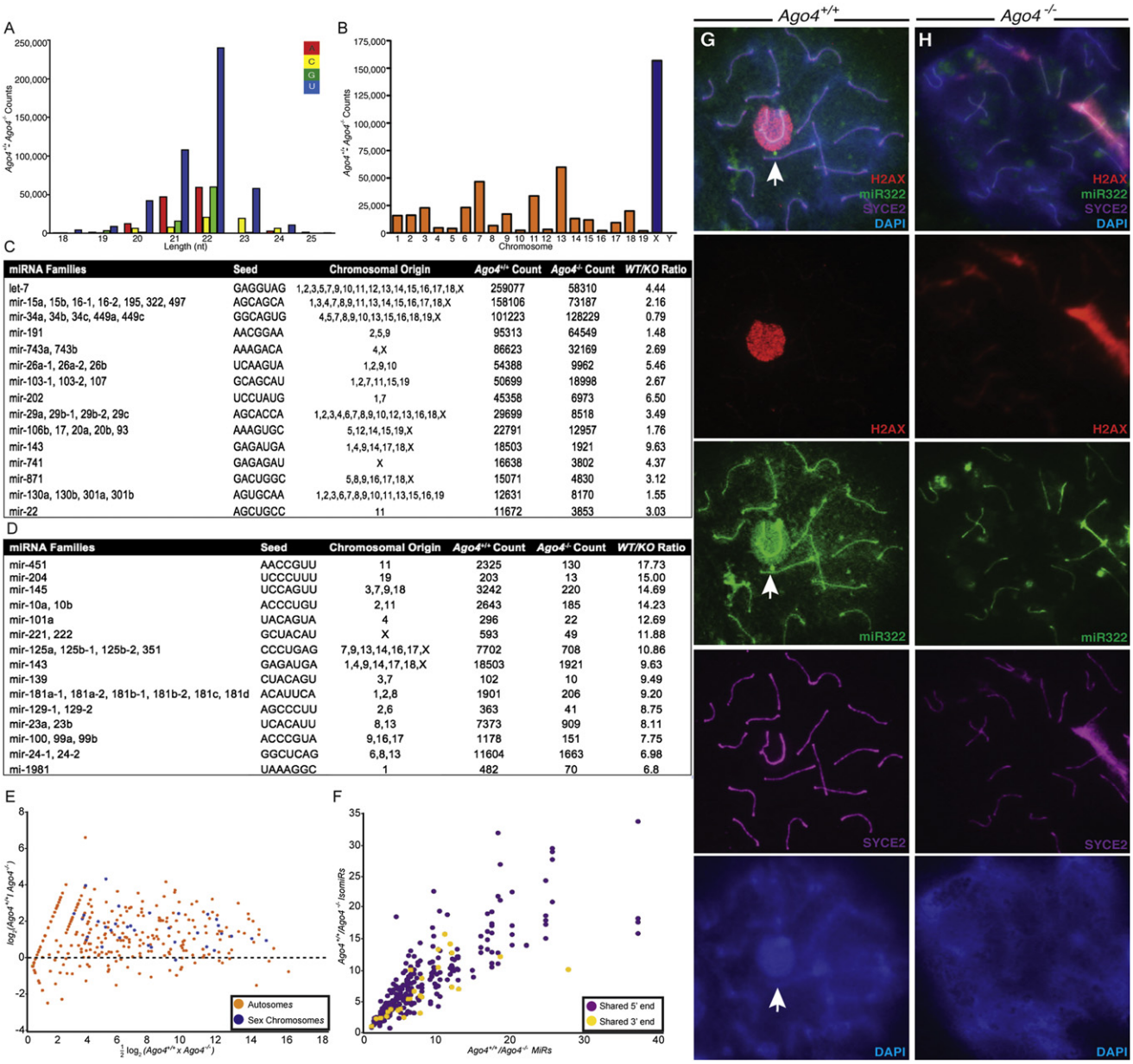

miRNA Families	Seed	Chromosomal Origin	*Ago4*$^{+/+}$ Count	*Ago4*$^{-/-}$ Count	*WT/KO* Ratio
let-7	GAGGUAG	1,2,3,5,7,9,10,11,12,13,14,15,16,17,18,X	259077	58310	4.44
mir-15a, 15b, 16-1, 16-2, 195, 322, 497	AGCAGCA	1,3,4,7,8,9,11,13,14,15,16,17,18,X	158106	73187	2.16
mir-34a, 34b, 34c, 449a, 449c	GGCAGUG	4,5,7,8,9,10,13,15,16,18,19,X	101223	128229	0.79
mir-191	AACGGAA	2,5,9	95313	64549	1.48
mir-743a, 743b	AAAGACA	4,X	86623	32169	2.69
mir-26a-1, 26a-2, 26b	UCAAGUA	1,2,9,10	54388	9962	5.46
mir-103-1, 103-2, 107	GCAGCAU	1,2,7,11,15,19	50699	18998	2.67
mir-202	UCCUAUG	1,7	45358	6973	6.50
mir-29a, 29b-1, 29b-2, 29c	AGCACCA	1,2,3,4,6,7,8,9,10,12,13,16,18,X	29699	8518	3.49
mir-106b, 17, 20a, 20b, 93	AAAGUGC	5,12,14,15,19,X	22791	12957	1.76
mir-143	GAGAUGA	1,4,9,14,17,18,X	18503	1921	9.63
mir-741	GAGAGAU	X	16638	3802	4.37
mir-871	GACUGGC	5,8,9,16,17,18,X	15071	4830	3.12
mir-130a, 130b, 301a, 301b	AGUGCAA	1,2,3,6,7,8,9,10,11,13,15,16,19	12631	8170	1.55
mir-22	AGCUGCC	11	11672	3853	3.03

miRNA Families	Seed	Chromosomal Origin	*Ago4*$^{+/+}$ Count	*Ago4*$^{-/-}$ Count	*WT/KO* Ratio
mir-451	AACCGUU	11	2325	130	17.73
mir-204	UCCCUUU	19	203	13	15.00
mir-145	UCCAGUU	3,7,9,18	3242	220	14.69
mir-10a, 10b	ACCCUGU	2,11	2643	185	14.23
mir-101a	UACAGUA	4	296	22	12.69
mir-221, 222	GCUACAU	X	593	49	11.88
mir-125a, 125b-1, 125b-2, 351	CCCUGAG	7,9,13,14,16,17,X	7702	708	10.86
mir-143	GAGAUGA	1,4,9,14,17,18,X	18503	1921	9.63
mir-139	CUACAGU	3,7	102	10	9.49
mir-181a-1, 181a-2, 181b-1, 181b-2, 181c, 181d	ACAUUCA	1,2,8	1901	206	9.20
mir-129-1, 129-2	AGCCCUU	2,6	363	41	8.75
mir-23a, 23b	UCACAUU	8,13	7373	909	8.11
mir-100, 99a, 99b	ACCCGUA	9,16,17	1178	151	7.75
mir-24-1, 24-2	GGCUCAG	6,8,13	11604	1663	6.98
mi-1981	UAAAGGC	1	482	70	6.8

Figure 4. Loss of *Ago4* Results in Loss of miRNAs Originating from Chromosome X and Wide-Scale Alterations in the Expression of Most miRNA Families

(A) The difference between miRNAs cloned from pachytene cells of WT and *Ago4*$^{-/-}$ males, distributed by miRNA length and base identity of the most 5′ nucleotide.

(B) For miRNAs with a single chromosomal origin, the difference between WT and mutant counts of these miRNAs is shown by chromosome (autosomes in orange; X chromosome in blue).

(C and D) miRNA families, grouped by common "seed" (nucleotides 2–7), with the highest expression in WT pachytene cells (C) and those showing the largest decrease in expression in the *Ago4*$^{-/-}$ (D).

(E) MA plot showing the intensity of expression (x axis) versus change in expression (y axis) for WT and mutant miRNAs reveals a preferential decrease in miRNA levels in the mutant for miRNAs originating from the sex chromosomes.

(F) Comparison of the ratio of WT to mutant miRNA counts between each miRNA and other variant species derived from the same hairpin.

(G and H) miRNA fluorescence in situ hybridization for miR-322 using pachytene stage spermatocytes from *Ago4*$^{+/+}$ (G) and *Ago4*$^{-/-}$ (H) mice stained with anti-γH2AX (red), anti-SYCE2 (purple), and DAPI (blue).

See also Figures S4 and S5 and Table S2.

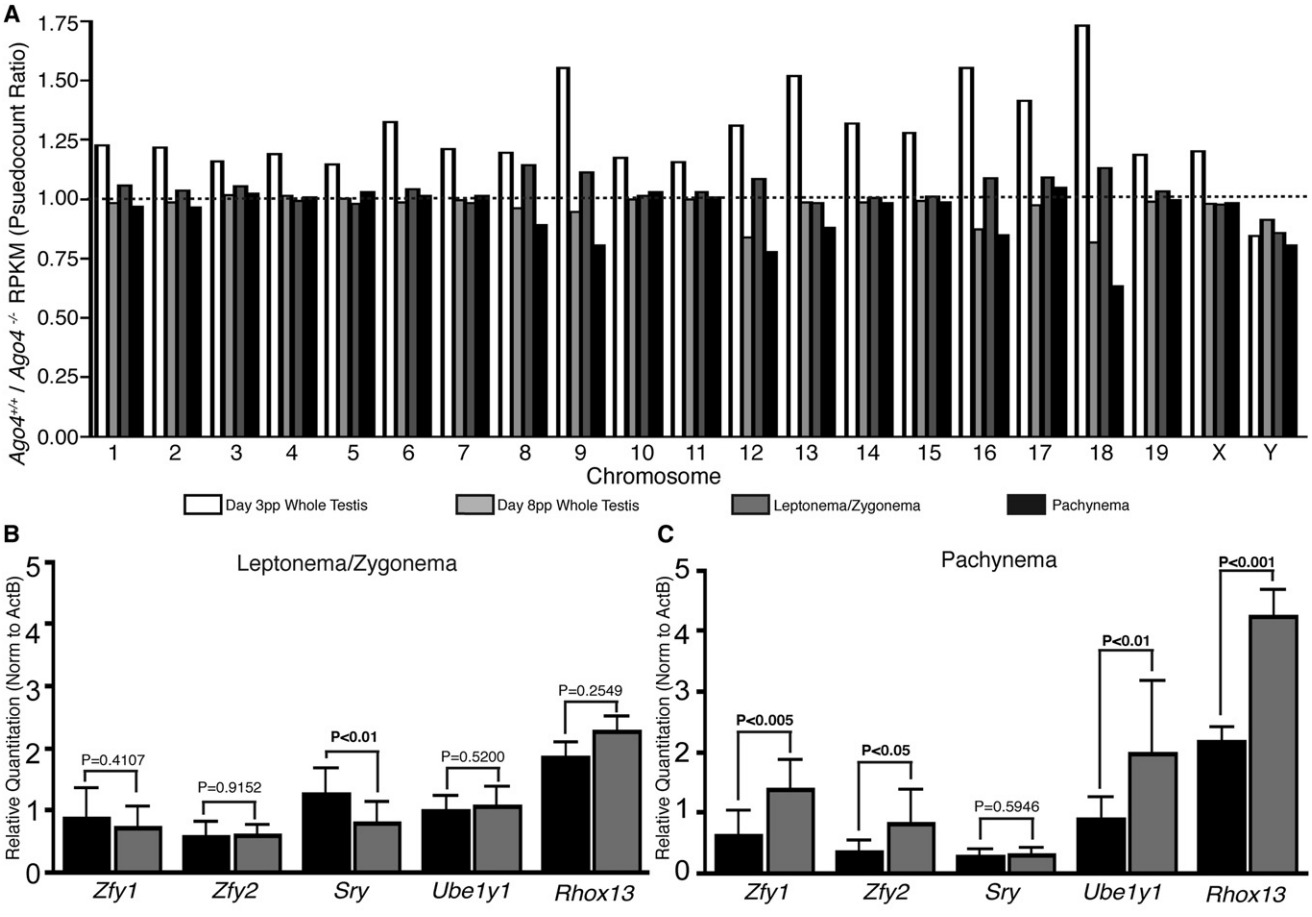

D

PreMeiotic Day 3 pp	p Value	PreMeiotic Day 8 pp	p Value	Leptonema/Zygonema	p Value	Pachynema	p Value
Gland morphogenesis	4.95×10^{-6}	M phase of meiotic cell cycle	1.35×10^{-5}	Cell motility	0.004583	Cell motion	7.53×10^{-6}
Amebodial cell migration	1.38×10^{-5}	Meiosis	1.35×10^{-5}	Localization of cell	0.004583	Heart development	0.012200
Positive regulation of gene expression	1.80×10^{-5}	Meiotic cell cycle	1.64×10^{-5}	Cell motion	0.012358	Cell motility	0.002326
Tube development	1.84×10^{-5}	Meiosis I	2.20×10^{-5}	Lymphocyte mediated immunity	0.014733	Localization of cell	0.002326
Epithelial tube morphogenesis	1.94×10^{-5}	Chromosome organization involved in meiosis	1.72×10^{-4}	Leukocyte adhesion	0.015524	Muscle organ development	0.005639
Epithelium development	1.99×10^{-5}	Synapsis	1.72×10^{-4}	Gene silencing	0.019912	Reproductive developmental process	0.006017
Morphogenesis of an epithelium	2.67×10^{-5}	Male meiosis	2.73×10^{-4}	Leukocyte mediated immunity	0.019912	Reproductive process in a multicellular organism	0.006049
Tube morphogenesis	3.57×10^{-5}	Synaptonemal complex assembly	3.96×10^{-4}	Adaptive immune response*	0.021371	Multicellular organism reproduction	0.006049
Positive regulation of macromolecule metabolic process	4.13×10^{-5}	Sister chromatid cohesion	3.96×10^{-4}	Adaptive immune response	0.021371	Sperm motility	0.008891
Positive regulation of RNA metabolic process	6.25×10^{-5}	Synaptonemal complex organization	5.58×10^{-4}	Regulation of cell motion	0.023741	Blood vessel morphogenesis	0.009230

Figure 5. RNAseq Profiling of Purified Spermatocytes from Different Stages of Prophase I and from Premeiotic Testes

(A) Differential expression between WT and *Ago4*$^{-/-}$ transcript levels was determined by RNAseq and depicted by ratios of WT to *Ago4*$^{-/-}$ mRNA levels by chromosome.

(B and C) Quantitative RT-PCR analysis of XY-linked gene expression in total RNA from isolated (B) leptotene/zygotene and (C) pachytene spermatocytes from *Ago4*$^{+/+}$ (n = 3, black bars) and *Ago4*$^{-/-}$ (n = 3, gray bars) adult littermates (significant values in bold). Error bars, SEM.

(D) GO analysis of transcripts showing significant differential expression ($q < 0.05$) in mRNA levels; the most significant groups of transcripts differentially expressed are shown for each cell type.

See also Table S3.

is the expression of these genes that results in meiotic arrest, rather than any effects of recombination failure per se (Royo et al., 2010). Importantly, RNAseq analysis of RNA from the leptotene/zygotene and pachytene stages did not show any differences in expression of *Atr* or *Brca1* between WT and mutant (Table S3). These genes are essential for phosphorylation of H2AX during MSCI (Turner et al., 2004), suggesting that the derepression of XY-linked genes is not due to failure to phosphorylate H2AX.

The derepression of certain XY-linked transcripts was examined further by performing quantitative reverse-transcription PCR on RNA from isolated leptotene/zygotene and pachytene spermatocytes (Figures 5B and 5C, respectively). Three out of four Y-linked genes examined (*Zfy1*, *Zfy2*, *Ube1y1*) and one X-linked gene (Rhox13) showed significant increases in expression in *Ago4*$^{-/-}$ spermatocytes compared to WT specifically at pachynema (Figure 5C), indicating that many XY-linked genes escape MSCI in the absence of AGO4.

Given our model for AGO4 involvement in MSCI, it was somewhat surprising to see only a modest loss of silencing in the SB, associated with modest persistence of ATR on the X, but not the Y, chromosome, and only a slight increase in ATR localization on the autosomes. This could reflect partial redundancy with AGO3, which is upregulated in *Ago4*$^{-/-}$ spermatocytes. Alternatively, this partial loss of MSCI could reflect the fact that only ~30% of cells observed in early pachynema have abnormal SB morphologies, which are likely eradicated by apoptosis; thus, those that survive are functionally intact with respect to MSCI processes. This possibility is supported by the finding that all abnormal SBs are observed in cells that are H1T negative, indicative of early pachynema, whereas only normal SB morphologies are observed in cells that are H1T positive, indicative of late pachynema.

Loss of *Ago4* Drives Premature Entry into Meiosis

While comparing gene expression profiles between *Ago4*$^{-/-}$ and WT littermate males, gene ontology (GO) analysis of RNAseq data revealed a dramatic upregulation of transcripts encoding proteins involved in spermatogonial proliferation in *Ago4*$^{-/-}$ testes on day 3–4 pp relative to WT, together with a distinct induction of genes regulating meiotic entry within day 8–9 pp *Ago4*$^{-/-}$ testes (Figure 5D). This suggests that loss of AGO4 facilitates spermatogonial differentiation and proliferation leading to premature meiotic initiation. In WT mice, meiotic initiation is brought about by the production of retinoic acid (RA) via the action of the RALDH2 enzyme (the product of the *Aldh1a2* gene) in Sertoli (and other) cells of the postnatal testis. The oxidation of RA by the P450 enzyme, CYP26B1, prevents RA-induced meiotic entry in fetal testes at a time when fetal oocytes initiate meiosis because they lack this enzyme (Hogarth and Griswold, 2010). In postnatal males, at around day 5–6 pp, RA binds to the retinoic acid receptor G (RARG) on the surface of type A spermatogonia (Gely-Pernot et al., 2012) and induces a cascade of genes, including *Stra8*, *Esco2*, and *Uba6* (Hogarth et al., 2011), whereas negative regulators of meiotic onset act to repress *Stra8* function and promote spermatogonial maintenance. These negative regulators of meiotic induction include *Nanos2* and *Fgf9* (Suzuki and Saga, 2008).

Genes involved in spermatogonial stem cell maintenance and proliferation were upregulated in RNA samples from day 3–4 pp *Ago4*$^{-/-}$ testes (Figure 6A). These included *Sox2* (Figure 6A) and *Sox9* (data not shown), members of the Sox family of transcription factors that are involved in the reactivation of stem cell pluripotency (Yabuta et al., 2006). Similarly, the RNA-binding protein, *Lin28b*, was upregulated along with its downstream target, *Prdm1*, whereas *let-7* was downregulated in *Ago4*$^{-/-}$ testes. Under the influence of RA, LIN28b is required to repress the somatic mesodermal program by sequestering the let-7 miRNA family, which in turn allows PRDM1 to act as an inducer of germ cell lineages (Bowles and Koopman, 2010). Thus, the day 3–4 pp GO analysis of RNA from whole *Ago4*$^{-/-}$ testes revealed a switch from spermatogonial stem cell maintenance to one of spermatogonial proliferation and/or differentiation.

At day 8–9 pp in *Ago4*$^{-/-}$ testes, *Cyp26b1*, *Nanos2*, and *Fgf9* levels are all reduced, whereas *Aldh1a2*, *Rarg*, and *Stra8* levels are greatly enhanced compared to *Ago4*$^{+/+}$ males. Similarly, *Esco2* and *Uba6* show premature increases in expression at day 8–9 pp in the *Ago4*$^{-/-}$ testes (Figure 6B). These alterations to transcripts involved in the induction of the RA pathway suggest that the absence of AGO4 results in premature induction of meiotic genes approximately 5 days earlier than in WT.

Early meiotic initiation in young *Ago4*$^{-/-}$ male pups was supported by the onset of expression of genes known to be essential and specific to meiotic prophase I, which usually occurs from around day 9 pp in the male mouse (Goetz et al., 1984). These include the genes encoding SPO11, the topoisomerase that generates DSBs that initiate meiotic recombination, the RecA homologs, DMC1 and RAD51, which process DSBs to facilitate homology searching and recombination (reviewed by Handel and Schimenti, 2010), TEX15, which facilitates loading of the RecA homologs (Yang et al., 2008), and the SC components, SYCP1 and SYCP3 (Figure 6C).

To confirm the early onset of prophase I at the cytological level, chromosome preps were examined from pups at days 5–6 and 8–9 pp. At day 5–6 pp, no cells were found to be in prophase I in *Ago4*$^{+/+}$ males, whereas a large number of cells from *Ago4*$^{-/-}$ males were found to be in preleptonema (data not shown). This difference was even more dramatic by day 8–9 pp, when large numbers of spermatocytes from *Ago4*$^{-/-}$ males were found to have entered, and progressed through, the early stages of prophase I. Progression through prophase I was demonstrated by staining with antibodies against SYCP3, together with SYCP1 (Figures 6D–6J), or with γH2AX (Figures 6K–6P), and with RAD51 (Figures 6Q–6V). In all cases, the major alteration to the spermatocyte pool in *Ago4*$^{-/-}$ males appeared to be a decrease in total leptotene cells (collective counts shown in Figure 6W, $n = 400$; $p < 0.005$, t test), and a concomitant increase in zygonema/pachynema intermediate cells ("Zyg/Pach" Figure 6W, $n = 400$; $p < 0.005$, t test). The emergence of pachytene cells in *Ago4*$^{-/-}$ males was approximately 5–6 days earlier than in WT males. Interestingly, all spermatocytes observed to reach the pachytene stage in the young mutant pups (Figures 6J and 6P) displayed defects identical to the altered staining patterns described earlier for spermatocytes from adult males. This observation suggests that meiotic progression in the adult can be partially rescued, perhaps by AGO3, whereas the initial waves of meiotic prophase I in early postnatal life are more wholly dependent on AGO4.

Together, our observations demonstrate early entry into meiosis in *Ago4*$^{-/-}$ males caused by premature induction of RA response genes that trigger meiotic initiation. These studies are in line with a recent report that demonstrates that the *C. elegans* Argonautes ALG-1 and ALG-2 are required for germ cell proliferation and entry into meiosis (Bukhari et al., 2012). In the worm, ALG-1 and ALG-2 localize to distal tip cells (DTCs), which are specialized somatic cells in the gonad that regulate the switch from mitosis to meiosis (Kimble and Crittenden, 2007), suggesting a cell-nonautonomous miRNA mechanism for regulating meiotic entry.

Conclusions

The studies described herein demonstrate a role for AGO4 in the nucleus of male germ cells. Our data support a model whereby AGO4-associated small RNAs directly participate in MSCI (Figure 7). Consistent with the discovery of nuclear RNAi components in human cells (Ahlenstiel et al., 2012; Robb et al., 2005),

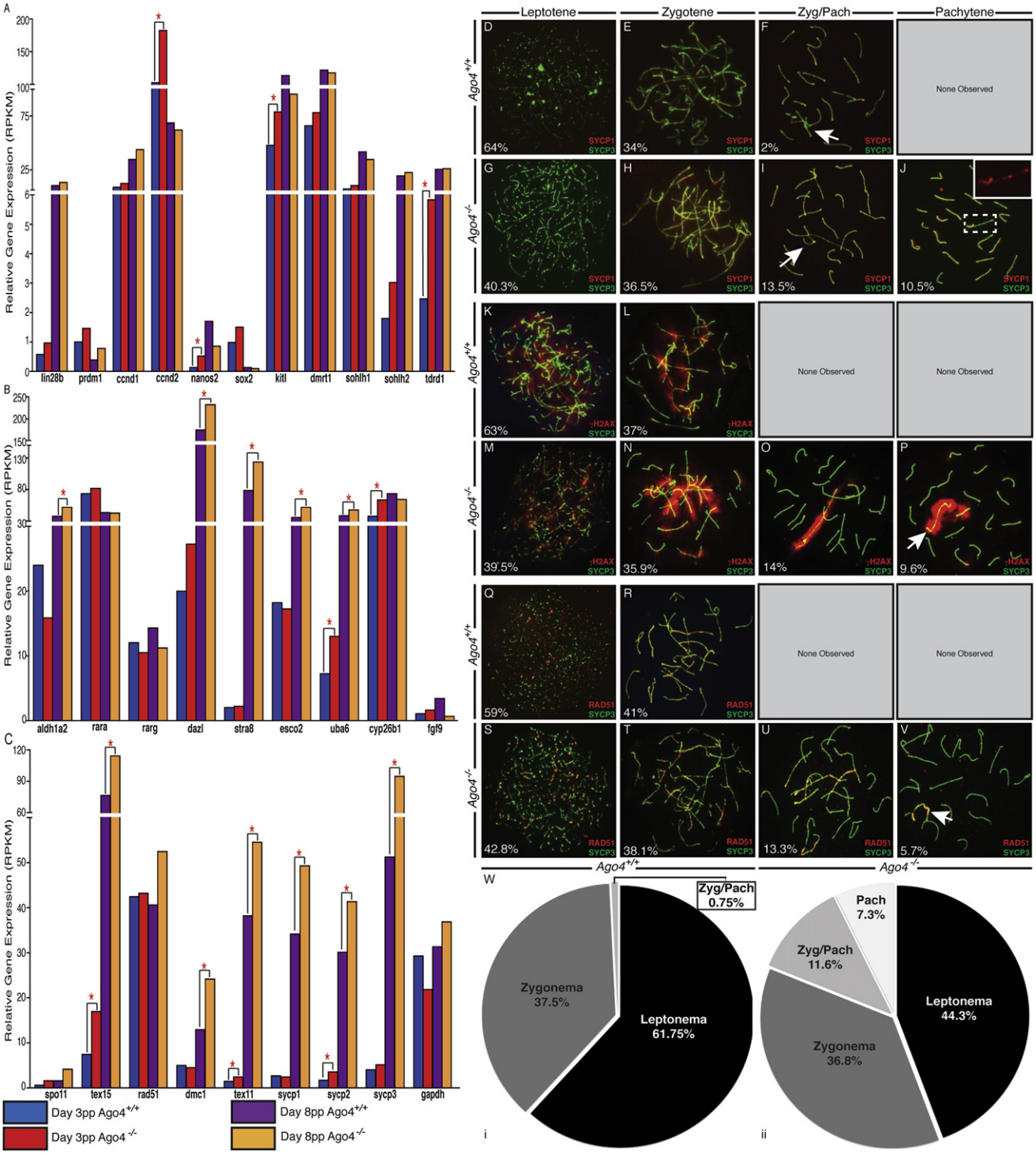

Figure 6. Loss of AGO4 Induces Early Entry into Meiosis in Postnatal Testes

(A–C) Quantification of transcripts from RNAseq performed on premeiotic testis from *Ago4*$^{+/+}$ and *Ago4*$^{-/-}$ males at day 3–4 pp (blue [*Ago4*$^{+/+}$] and red [*Ago4*$^{-/-}$] bars) and day 8–9 pp (purple [*Ago4*$^{+/+}$] and orange [*Ago4*$^{-/-}$] bars). GAPDH is shown as a control. Genes with a significant degree of differential expression between *Ago4*$^{+/+}$ and *Ago4*$^{-/-}$ males ($q < 0.05$) are indicated with an asterisk (*). Genes in (A) are associated with spermatogonial proliferation and/or differentiation. Genes in (B) are involved in the initiation of meiosis, via RA. Genes involved in early prophase I progression are in (C).

(D–V) Chromosome immunofluorescence from day 8–9 pp testes from *Ago4*$^{+/+}$ (D–F, K, L, Q, R, and Wi) and *Ago4*$^{-/-}$ (G–J, M–P, S–V, and Wii) littermates stained with anti-SYCP3 (green), together with anti-SYCP1 (D–J), anti-γH2AX (K–P), or anti-RAD51 (Q–V), all in red. Progression through prophase I is depicted by

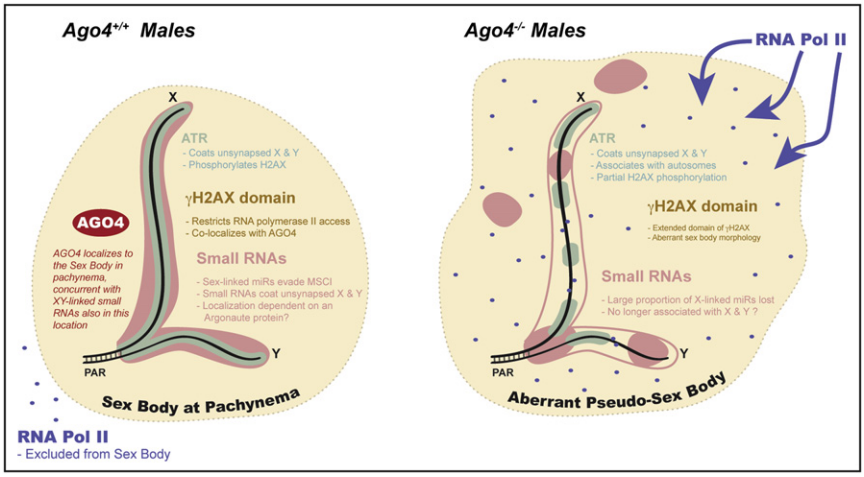

Figure 7. Model for the Role of AGO4 in Meiotic Silencing

In WT males at pachynema (left side), the SB domain is defined by localization of γH2AX (yellow background), whose phosphorylation is mediated by the ATR kinase, which coats the unsynapsed lengths of the X and Y chromosomes (green). Sex chromosomes are also coated with small RNAs (pink) at this time. We propose that the presence of these RNA species may depend on AGO4, and the sum effect is the exclusion of RNAP II from the SB and silencing of the sex chromosomes by MSCI. In the absence of AGO4 (right side), ATR localization is drastically reduced along abnormal SB morphology. Sex-linked small RNAs are drastically reduced and no longer reside in the SB, leading to RNAP II infiltration and failed silencing. These effects are distinct from those involving RA signaling and meiotic initiation described in Figure 6.

our study reveals distinct localization patterns for both AGO3 and AGO4 within the nuclei of mouse spermatogenic cells, along with certain miRNAs. These observations support the idea that AGO4 may recruit small RNAs to the SB, or vice versa. Importantly, we show that in the absence of AGO4, disproportionate numbers of downregulated miRNAs originate from the X chromosome and that miRNA localization in the SB is markedly reduced. This loss of miRNAs specifically from X and Y is contrary to expectation, given the increased localization of RNAP II in the SB, but is in line with the fact that X-linked miRNAs have been found to escape repression during MSCI of prophase I (Song et al., 2009).

Given the localization of AGO4 to asynapsed regions and the SB in pachynema, together with its colocalization with mediators of MSCI (ATR and γH2AX), and the dependence of these mediators on AGO4, the results presented herein indicate a role for AGO4 in the initiation and/or maintenance of transcriptional silencing during prophase I. We hypothesize that this transcriptional regulation is regulated by AGO4 in a manner reminiscent of the RITS complex seen in *S. pombe* and *C. elegans* (van Wolfswinkel and Ketting, 2010). Although small RNAs have been postulated to be involved in MSCI (Burgoyne et al., 2009), our data provide direct evidence for AGO4 in these events (Figure 7).

The role of AGO4 in meiotic initiation appears to originate in at least two cell types: the RA-producing Sertoli cells, and the spermatogonia. However, AGO4 expression appears to be confined to the germ lineages, leading us to postulate an indirect effect on RA production by the somatic cells of the testis. In this scenario, loss of AGO4 results in loss of a signal from the germ cells to the Sertoli cells that would usually repress RA production. The action of AGO4 in the germ cells themselves may be directed toward RA signal transduction and/or toward downstream mediators. Indeed, treatment of fetal testes with trichostatin A, an inhibitor of class I/II histone deacetylases, promotes premature activation of *Stra8* expression and early meiotic entry (Wang and Tilly, 2010), suggesting epigenetic regulation of these events. Moreover, there is evidence supporting the role of RNA-binding proteins and small RNAs in self-renewal of spermatogonial stem cells (Niu et al., 2011), as well as in the response of spermatogonia to RA signaling (Griswold et al., 2012; Ro et al., 2007). For example, DAZL, an RNA-binding protein expressed in germ cells, which is upregulated on day 8–9 pp in the absence of AGO4, facilitates germ cell responses to RA to promote meiotic initiation (Gill et al., 2011; Lin et al., 2008; Lin and Page, 2005). In contrast, two miRNA clusters have been implicated during spermatogonial differentiation in mice, *miR-17-92* and *miR-106b-25* (Tong et al., 2011), and both are downregulated in *Ago4*$^{-/-}$ testes.

Taken together, our studies demonstrate important roles for AGO4 in meiotic induction and progression in male mice. Of particular note is the observation that AGO4 is found in the nucleus of prophase I cells, suggesting the existence of a RITS-like complex at the level of heterochromatin during meiosis. Finally, it is important to note that the two roles for AGO4 in mammalian germ cells that we describe appear to be distinct because treatment of vitamin A-deficient mice with RA does not lead to MSCI defects or meiotic disruption (van Pelt and de Rooij, 1990). Indeed, it is plausible that the early meiotic entry and the MSCI events require different roles for AGO4 in the context of its nuclear and cytoplasmic activities. Continued studies are aimed at elucidating the mechanisms of AGO4 involvement in these mammalian germ cell events.

EXPERIMENTAL PROCEDURES

Generation of Ago4 Mutant Mice

All mouse studies were conducted with the prior approval of the Cornell Institutional Animal Care and Use Committee. An *Ago4*-targeting construct, containing a 2.5 kbp 5′ arm from intron 2 of *Ago4*, a LoxP site, 25.4 kb of *Ago4* from exons 3–17, an *Frt*-flanked *Pgk-neo* cassette, a second LoxP site, and a 1.6 kbp 3′ arm within intron 17 of Ago4 (Figures S1D–S1F), was used to generate chimeric mice using standard mouse mutagenesis techniques. Following FlpE and CRE-mediated excision of the *Frt*-flanked and

horizontal panels from left to right. If no image is given for a particular stage of prophase I, then that stage was not observed in the staining for this genotype. Percent (%) cells found at each stage is shown.
(Wi and Wii) Quantification of prophase I stages for *Ago4*$^{+/+}$ and *Ago4*$^{-/-}$, respectively (n = 400). χ^2 analysis revealed significant differences between the two populations (***p < 0.0001).

LoxP-flanked cassettes, respectively, the resulting *Ago4*$^{-/-}$ allele (lacking exons 3–17) was bred to homozygosity onto a C57BL/6 background.

Testes Weights, Sperm Counts, and Histology

Whole testes were removed from *Ago4*$^{+/+}$ and *Ago4*$^{-/-}$ littermates and weighed, and epididymal sperm counts assessed (Edelmann et al., 1996). For histological analysis, testes were fixed in Bouin's (for H&E) or in 10% formalin (for all other staining and for TUNEL) overnight at 4°C. Paraffin-embedded tissues were sectioned at 5 μm before dewaxing and histological staining.

Chromosome Spreading and Immunofluorescent Staining

Prophase I chromosome spreads and antibody staining were prepared as previously described (Holloway et al., 2008; Holloway et al., 2011; Kolas et al., 2005; Lipkin et al., 2002) using antibodies from various sources (see Supplemental Experimental Procedures).

RT-PCR and Quantitative PCR

Total RNA was extracted from whole tissue or isolated spermatocytes using TRIzol reagent (Invitrogen). Reverse transcription was performed using SuperScript III (Invitrogen). For real-time PCR analysis, TaqMan probes (Applied Biosystems, Carlsbad CA, USA) were used on the 7500 Real-Time PCR System (Applied Biosystems). Raw data were analyzed using the 7500 System Sequence Detection Software (Applied Biosystems). Probe sets are provided in Supplemental Experimental Procedures.

Isolation of Mouse Spermatogenic Cells

Testes from adult *Ago4*$^{+/+}$ and *Ago4*$^{-/-}$ mice (day 70–80 pp) were removed, weighed, and decapsulated prior to enrichment of specific spermatogenic cell types using the STA-PUT method based on separation by cell diameter/density at unit gravity (Bellvé, 1993). Purity of resulting fractions was determined by microscopy based on cell diameter and morphology. Pachytene cells were at approximately 95% purification with potential contamination from spermatocytes of slightly earlier or later developmental timing.

mRNA Transcript Sequencing and Analysis

mRNA transcripts were isolated and prepared for sequencing using Illumina's TruSeq kit. The completed library was sequenced on an Illumina HiSeq 2000 and aligned to the genome using TopHat and Cuffdiff programs (Trapnell et al., 2009) to determine differential expression between WT and mutant samples. A q value, which represents a false discovery rate-corrected p value (Klipper-Aurbach et al., 1995), of <0.05 was chosen as the cutoff for determining whether differential gene expression was significant. For ontology analysis, genes with significant differential expression were analyzed using DAVID (Huang et al., 2009a, 2009b).

Small RNA Sequencing and Analysis

Small RNA sequencing was performed as described previously (Grimson et al., 2008). Sequences were filtered to remove reads containing undefined bases ("N") and reads under 14 nt in length. Sequences were aligned to the genome using Bowtie (version 0.12.07; Langmead et al., 2009). miRNAs were determined by alignment of sequences to mouse miRNA hairpins (miRBase Release 18; Griffiths-Jones, 2004; Griffiths-Jones et al., 2006, 2008).

miRNA Fluorescent In Situ Hybridization and Immunofluorescence

Slides were prepared and stained as described above with modifications to retain RNA (see Supplemental Experimental Procedures). Following immunofluorescence with primary antibodies as described previously (Holloway et al., 2010; Kolas et al., 2005), and using an anti-SYCE2 antibody (from Howard Cooke, Edinburgh, Scotland), fluorescein-conjugated Locked Nucleic Acid (LNA) probes (Exiqon, Copenhagen, Denmark) were used to probe for mature miRNA localization. Probes were first denatured by incubation at 90°C for 4 min, and hybridizations were carried out at the appropriate incubation temperature overnight. Slides were then washed, mounted with antifade (ProLong Gold; Molecular Probes), and visualized.

ACCESSION NUMBERS

The GEO accession number for the small RNA and mRNA Illumina sequence reported in this paper is GSE39652.

SUPPLEMENTAL INFORMATION

Supplemental Information includes five figures, three tables, and Supplemental Experimental Procedures and can be found with this article online at http://dx.doi.org/10.1016/j.devcel.2012.07.003.

ACKNOWLEDGMENTS

This work was supported by the Vertebrate Genomics Center at Cornell University (VERGE postdoctoral award to R.J.H. and predoctoral award to S.H.) and by funding from the NIH to P.E.C. (HD041012). A.J.M. was supported by NIH training grants in Genetics and Development (T32GM00761) and in Reproductive Genomics (T32HD052471); S.H. was supported by an NIH training grant in Biochemistry, Molecular and Cellular Biology. The authors acknowledge with gratitude the generosity of Dr. Mary Ann Handel (The Jackson Laboratory) for providing the anti-H1T antibody, Dr. Raimundo Freire (Tenerife, Spain) for providing the anti-TOPBP1 antibody, Drs. Ian Adams and Howard Cooke (University of Edinburgh, Scotland) for providing the anti-SYCE2 antibody, and Dr. George Enders (University of Kansas Medical Center) for providing the GCNA1 hybridoma supernatant. We are grateful to Ian Welsh for technical advice and to Ewelina Bolcun-Filas, Jen Grenier, Kim Holloway, and Mark Roberson for reading this manuscript and for helpful suggestions. We also thank Kim Holloway for extensive guidance in preparing figures and editorial assistance. We thank Peter L. Borst for assistance in mouse care.

Received: March 12, 2012
Revised: June 9, 2012
Accepted: July 5, 2012
Published online: August 2, 2012

REFERENCES

Ahlenstiel, C.L., Lim, H.G., Cooper, D.A., Ishida, T., Kelleher, A.D., and Suzuki, K. (2012). Direct evidence of nuclear Argonaute distribution during transcriptional silencing links the actin cytoskeleton to nuclear RNAi machinery in human cells. Nucleic Acids Res. *40*, 1579–1595.

Aravin, A., Gaidatzis, D., Pfeffer, S., Lagos-Quintana, M., Landgraf, P., Iovino, N., Morris, P., Brownstein, M.J., Kuramochi-Miyagawa, S., Nakano, T., et al. (2006). A novel class of small RNAs bind to MILI protein in mouse testes. Nature *442*, 203–207.

Baarends, W.M., and Grootegoed, J.A. (2003). Chromatin dynamics in the male meiotic prophase. Cytogenet. Genome Res. *103*, 225–234.

Baarends, W.M., Wassenaar, E., van der Laan, R., Hoogerbrugge, J., Sleddens-Linkels, E., Hoeijmakers, J.H., de Boer, P., and Grootegoed, J.A. (2005). Silencing of unpaired chromatin and histone H2A ubiquitination in mammalian meiosis. Mol. Cell. Biol. *25*, 1041–1053.

Barchi, M., Mahadevaiah, S., Di Giacomo, M., Baudat, F., de Rooij, D.G., Burgoyne, P.S., Jasin, M., and Keeney, S. (2005). Surveillance of different recombination defects in mouse spermatocytes yields distinct responses despite elimination at an identical developmental stage. Mol. Cell. Biol. *25*, 7203–7215.

Bellani, M.A., Romanienko, P.J., Cairatti, D.A., and Camerini-Otero, R.D. (2005). SPO11 is required for sex-body formation, and Spo11 heterozygosity rescues the prophase arrest of Atm-/- spermatocytes. J. Cell Sci. *118*, 3233–3245.

Bellvé, A.R. (1993). Purification, culture, and fractionation of spermatogenic cells. Methods Enzymol. *225*, 84–113.

Bowles, J., and Koopman, P. (2010). Sex determination in mammalian germ cells: extrinsic versus intrinsic factors. Reproduction *139*, 943–958.

Brown, P.W., Hwang, K., Schlegel, P.N., and Morris, P.L. (2008). Small ubiquitin-related modifier (SUMO)-1, SUMO-2/3 and SUMOylation are

involved with centromeric heterochromatin of chromosomes 9 and 1 and proteins of the synaptonemal complex during meiosis in men. Hum. Reprod. *23*, 2850–2857.

Bukhari, S.I., Vasquez-Rifo, A., Gagné, D., Paquet, E.R., Zetka, M., Robert, C., Masson, J.Y., and Simard, M.J. (2012). The microRNA pathway controls germ cell proliferation and differentiation in *C. elegans*. Cell Res. *22*, 1034–1045.

Burgoyne, P.S., Mahadevaiah, S.K., and Turner, J.M. (2009). The consequences of asynapsis for mammalian meiosis. Nat. Rev. Genet. *10*, 207–216.

Cenik, E.S., and Zamore, P.D. (2011). Argonaute proteins. Curr. Biol. *21*, R446–R449.

Czech, B., and Hannon, G.J. (2011). Small RNA sorting: matchmaking for Argonautes. Nat. Rev. Genet. *12*, 19–31.

Daniel, K., Lange, J., Hached, K., Fu, J., Anastassiadis, K., Roig, I., Cooke, H.J., Stewart, A.F., Wassmann, K., Jasin, M., et al. (2011). Meiotic homologue alignment and its quality surveillance are controlled by mouse HORMAD1. Nat. Cell Biol. *13*, 599–610.

Edelmann, W., Cohen, P.E., Kane, M., Lau, K., Morrow, B., Bennett, S., Umar, A., Kunkel, T., Cattoretti, G., Chaganti, R., et al. (1996). Meiotic pachytene arrest in MLH1-deficient mice. Cell *85*, 1125–1134.

Fernandez-Capetillo, O., Mahadevaiah, S.K., Celeste, A., Romanienko, P.J., Camerini-Otero, R.D., Bonner, W.M., Manova, K., Burgoyne, P., and Nussenzweig, A. (2003). H2AX is required for chromatin remodeling and inactivation of sex chromosomes in male mouse meiosis. Dev. Cell *4*, 497–508.

Gely-Pernot, A., Raverdeau, M., Célébi, C., Dennefeld, C., Feret, B., Klopfenstein, M., Yoshida, S., Ghyselinck, N.B., and Mark, M. (2012). Spermatogonia differentiation requires retinoic acid receptor γ. Endocrinology *153*, 438–449.

Gill, M.E., Hu, Y.C., Lin, Y., and Page, D.C. (2011). Licensing of gametogenesis, dependent on RNA binding protein DAZL, as a gateway to sexual differentiation of fetal germ cells. Proc. Natl. Acad. Sci. USA *108*, 7443–7448.

Girard, A., Sachidanandam, R., Hannon, G.J., and Carmell, M.A. (2006). A germline-specific class of small RNAs binds mammalian Piwi proteins. Nature *442*, 199–202.

Goetz, P., Chandley, A.C., and Speed, R.M. (1984). Morphological and temporal sequence of meiotic prophase development at puberty in the male mouse. J. Cell Sci. *65*, 249–263.

González-González, E., López-Casas, P.P., and del Mazo, J. (2008). The expression patterns of genes involved in the RNAi pathways are tissue-dependent and differ in the germ and somatic cells of mouse testis. Biochim. Biophys. Acta *1779*, 306–311.

Griffiths-Jones, S. (2004). The microRNA Registry. Nucleic Acids Res. *32* (Database issue), D109–D111.

Griffiths-Jones, S., Grocock, R.J., van Dongen, S., Bateman, A., and Enright, A.J. (2006). miRBase: microRNA sequences, targets and gene nomenclature. Nucleic Acids Res. *34* (Database issue), D140–D144.

Griffiths-Jones, S., Saini, H.K., van Dongen, S., and Enright, A.J. (2008). miRBase: tools for microRNA genomics. Nucleic Acids Res. *36* (Database issue), D154–D158.

Grimson, A., Srivastava, M., Fahey, B., Woodcroft, B.J., Chiang, H.R., King, N., Degnan, B.M., Rokhsar, D.S., and Bartel, D.P. (2008). Early origins and evolution of microRNAs and Piwi-interacting RNAs in animals. Nature *455*, 1193–1197.

Griswold, M.D., Hogarth, C.A., Bowles, J., and Koopman, P. (2012). Initiating meiosis: the case for retinoic acid. Biol. Reprod. *86*, 35.

Grivna, S.T., Beyret, E., Wang, Z., and Lin, H. (2006). A novel class of small RNAs in mouse spermatogenic cells. Genes Dev. *20*, 1709–1714.

Handel, M.A. (2004). The XY body: a specialized meiotic chromatin domain. Exp. Cell Res. *296*, 57–63.

Handel, M.A., and Schimenti, J.C. (2010). Genetics of mammalian meiosis: regulation, dynamics and impact on fertility. Nat. Rev. Genet. *11*, 124–136.

Hogarth, C.A., and Griswold, M.D. (2010). The key role of vitamin A in spermatogenesis. J. Clin. Invest. *120*, 956–962.

Hogarth, C.A., Mitchell, D., Evanoff, R., Small, C., and Griswold, M. (2011). Identification and expression of potential regulators of the mammalian mitotic-to-meiotic transition. Biol. Reprod. *84*, 34–42.

Holloway, J.K., Booth, J., Edelmann, W., McGowan, C.H., and Cohen, P.E. (2008). MUS81 generates a subset of MLH1-MLH3-independent crossovers in mammalian meiosis. PLoS Genet. *4*, e1000186.

Holloway, J.K., Morelli, M.A., Borst, P.L., and Cohen, P.E. (2010). Mammalian BLM helicase is critical for integrating multiple pathways of meiotic recombination. J. Cell Biol. *188*, 779–789.

Holloway, J.K., Mohan, S., Balmus, G., Sun, X., Modzelewski, A., Borst, P.L., Freire, R., Weiss, R.S., and Cohen, P.E. (2011). Mammalian BTBD12 (SLX4) protects against genomic instability during mammalian spermatogenesis. PLoS Genet. *7*, e1002094.

Huang, da W., Sherman, B.T., and Lempicki, R.A. (2009a). Bioinformatics enrichment tools: paths toward the comprehensive functional analysis of large gene lists. Nucleic Acids Res. *37*, 1–13.

Huang, da W., Sherman, B.T., and Lempicki, R.A. (2009b). Systematic and integrative analysis of large gene lists using DAVID bioinformatics resources. Nat. Protoc. *4*, 44–57.

Kim, D.H., Villeneuve, L.M., Morris, K.V., and Rossi, J.J. (2006). Argonaute-1 directs siRNA-mediated transcriptional gene silencing in human cells. Nat. Struct. Mol. Biol. *13*, 793–797.

Kim, S., Namekawa, S.H., Niswander, L.M., Ward, J.O., Lee, J.T., Bardwell, V.J., and Zarkower, D. (2007). A mammal-specific Doublesex homolog associates with male sex chromatin and is required for male meiosis. PLoS Genet. *3*, e62.

Kimble, J., and Crittenden, S.L. (2007). Controls of germline stem cells, entry into meiosis, and the sperm/oocyte decision in *Caenorhabditis elegans*. Annu. Rev. Cell Dev. Biol. *23*, 405–433.

Klipper-Aurbach, Y., Wasserman, M., Braunspiegel-Weintrob, N., Borstein, D., Peleg, S., Assa, S., Karp, M., Benjamini, Y., Hochberg, Y., and Laron, Z. (1995). Mathematical formulae for the prediction of the residual beta cell function during the first two years of disease in children and adolescents with insulin-dependent diabetes mellitus. Med. Hypotheses *45*, 486–490.

Kolas, N.K., Svetlanov, A., Lenzi, M.L., Macaluso, F.P., Lipkin, S.M., Liskay, R.M., Greally, J., Edelmann, W., and Cohen, P.E. (2005). Localization of MMR proteins on meiotic chromosomes in mice indicates distinct functions during prophase I. J. Cell Biol. *171*, 447–458.

Kumagai, A., Lee, J., Yoo, H.Y., and Dunphy, W.G. (2006). TopBP1 activates the ATR-ATRIP complex. Cell *124*, 943–955.

Langmead, B., Trapnell, C., Pop, M., and Salzberg, S.L. (2009). Ultrafast and memory-efficient alignment of short DNA sequences to the human genome. Genome Biol. *10*, R25.

Lin, Q., Sirotkin, A., and Skoultchi, A.I. (2000). Normal spermatogenesis in mice lacking the testis-specific linker histone H1t. Mol. Cell. Biol. *20*, 2122–2128.

Lin, Y., and Page, D.C. (2005). Dazl deficiency leads to embryonic arrest of germ cell development in XY C57BL/6 mice. Dev. Biol. *288*, 309–316.

Lin, Y., Gill, M.E., Koubova, J., and Page, D.C. (2008). Germ cell-intrinsic and -extrinsic factors govern meiotic initiation in mouse embryos. Science *322*, 1685–1687.

Lipkin, S.M., Moens, P.B., Wang, V., Lenzi, M., Shanmugarajah, D., Gilgeous, A., Thomas, J., Cheng, J., Touchman, J.W., Green, E.D., et al. (2002). Meiotic arrest and aneuploidy in MLH3-deficient mice. Nat. Genet. *31*, 385–390.

Liu, J., Carmell, M.A., Rivas, F.V., Marsden, C.G., Thomson, J.M., Song, J.J., Hammond, S.M., Joshua-Tor, L., and Hannon, G.J. (2004). Argonaute2 is the catalytic engine of mammalian RNAi. Science *305*, 1437–1441.

Maine, E.M. (2010). Meiotic silencing in *Caenorhabditis elegans*. Int. Rev. Cell Mol. Biol. *282*, 91–134.

Marcon, E., Babak, T., Chua, G., Hughes, T., and Moens, P.B. (2008). miRNA and piRNA localization in the male mammalian meiotic nucleus. Chromosome Res. *16*, 243–260.

Meister, G., Landthaler, M., Patkaniowska, A., Dorsett, Y., Teng, G., and Tuschl, T. (2004). Human Argonaute2 mediates RNA cleavage targeted by miRNAs and siRNAs. Mol. Cell *15*, 185–197.

Niu, Z., Goodyear, S.M., Rao, S., Wu, X., Tobias, J.W., Avarbock, M.R., and Brinster, R.L. (2011). MicroRNA-21 regulates the self-renewal of mouse spermatogonial stem cells. Proc. Natl. Acad. Sci. USA *108*, 12740–12745.

Okamura, K., Liu, N., and Lai, E.C. (2009). Distinct mechanisms for microRNA strand selection by *Drosophila* Argonautes. Mol. Cell *36*, 431–444.

Pillai, R.S., and Chuma, S. (2012). piRNAs and their involvement in male germline development in mice. Dev. Growth Differ. Published online January 6, 2012. http://dx.doi.org/10.1111/j.1440-169X.2011.01320.x.

Raju, N.B., Metzenberg, R.L., and Shiu, P.K. (2007). Neurospora spore killers Sk-2 and Sk-3 suppress meiotic silencing by unpaired DNA. Genetics *176*, 43–52.

Ro, S., Park, C., Sanders, K.M., McCarrey, J.R., and Yan, W. (2007). Cloning and expression profiling of testis-expressed microRNAs. Dev. Biol. *311*, 592–602.

Robb, G.B., Brown, K.M., Khurana, J., and Rana, T.M. (2005). Specific and potent RNAi in the nucleus of human cells. Nat. Struct. Mol. Biol. *12*, 133–137.

Royo, H., Polikiewicz, G., Mahadevaiah, S.K., Prosser, H., Mitchell, M., Bradley, A., de Rooij, D.G., Burgoyne, P.S., and Turner, J.M. (2010). Evidence that meiotic sex chromosome inactivation is essential for male fertility. Curr. Biol. *20*, 2117–2123.

Ruby, J.G., Jan, C., Player, C., Axtell, M.J., Lee, W., Nusbaum, C., Ge, H., and Bartel, D.P. (2006). Large-scale sequencing reveals 21U-RNAs and additional microRNAs and endogenous siRNAs in *C. elegans*. Cell *127*, 1193–1207.

Ruby, J.G., Stark, A., Johnston, W.K., Kellis, M., Bartel, D.P., and Lai, E.C. (2007). Evolution, biogenesis, expression, and target predictions of a substantially expanded set of *Drosophila* microRNAs. Genome Res. *17*, 1850–1864.

Schimenti, J. (2005). Synapsis or silence. Nat. Genet. *37*, 11–13.

Shiu, P.K., Raju, N.B., Zickler, D., and Metzenberg, R.L. (2001). Meiotic silencing by unpaired DNA. Cell *107*, 905–916.

Siomi, M.C., Sato, K., Pezic, D., and Aravin, A.A. (2011). PIWI-interacting small RNAs: the vanguard of genome defence. Nat. Rev. Mol. Cell Biol. *12*, 246–258.

Song, J.J., Liu, J., Tolia, N.H., Schneiderman, J., Smith, S.K., Martienssen, R.A., Hannon, G.J., and Joshua-Tor, L. (2003). The crystal structure of the Argonaute2 PAZ domain reveals an RNA binding motif in RNAi effector complexes. Nat. Struct. Biol. *10*, 1026–1032.

Song, R., Ro, S., Michaels, J.D., Park, C., McCarrey, J.R., and Yan, W. (2009). Many X-linked microRNAs escape meiotic sex chromosome inactivation. Nat. Genet. *41*, 488–493.

Song, R., Hennig, G.W., Wu, Q., Jose, C., Zheng, H., and Yan, W. (2011). Male germ cells express abundant endogenous siRNAs. Proc. Natl. Acad. Sci. USA *108*, 13159–13164.

Steiner, F.A., and Plasterk, R.H. (2006). Knocking out the Argonautes. Cell *127*, 667–668.

Suzuki, A., and Saga, Y. (2008). Nanos2 suppresses meiosis and promotes male germ cell differentiation. Genes Dev. *22*, 430–435.

Tachibana, M., Nozaki, M., Takeda, N., and Shinkai, Y. (2007). Functional dynamics of H3K9 methylation during meiotic prophase progression. EMBO J. *26*, 3346–3359.

Tong, M.H., Mitchell, D., Evanoff, R., and Griswold, M.D. (2011). Expression of Mirlet7 family microRNAs in response to retinoic acid-induced spermatogonial differentiation in mice. Biol. Reprod. *85*, 189–197.

Trapnell, C., Pachter, L., and Salzberg, S.L. (2009). TopHat: discovering splice junctions with RNA-Seq. Bioinformatics *25*, 1105–1111.

Turner, J.M. (2007). Meiotic sex chromosome inactivation. Development *134*, 1823–1831.

Turner, J.M., Aprelikova, O., Xu, X., Wang, R., Kim, S., Chandramouli, G.V., Barrett, J.C., Burgoyne, P.S., and Deng, C.X. (2004). BRCA1, histone H2AX phosphorylation, and male meiotic sex chromosome inactivation. Curr. Biol. *14*, 2135–2142.

Turner, J.M., Mahadevaiah, S.K., Fernandez-Capetillo, O., Nussenzweig, A., Xu, X., Deng, C.X., and Burgoyne, P.S. (2005). Silencing of unsynapsed meiotic chromosomes in the mouse. Nat. Genet. *37*, 41–47.

van Pelt, A.M., and de Rooij, D.G. (1990). Synchronization of the seminiferous epithelium after vitamin A replacement in vitamin A-deficient mice. Biol. Reprod. *43*, 363–367.

van Wolfswinkel, J.C., and Ketting, R.F. (2010). The role of small non-coding RNAs in genome stability and chromatin organization. J. Cell Sci. *123*, 1825–1839.

Vigodner, M. (2009). Sumoylation precedes accumulation of phosphorylated H2AX on sex chromosomes during their meiotic inactivation. Chromosome Res. *17*, 37–45.

Wang, H., Zhang, X., Liu, J., Kiba, T., Woo, J., Ojo, T., Hafner, M., Tuschl, T., Chua, N.H., and Wang, X.J. (2011). Deep sequencing of small RNAs specifically associated with *Arabidopsis* AGO1 and AGO4 uncovers new AGO functions. Plant J. *67*, 292–304.

Wang, N., and Tilly, J.L. (2010). Epigenetic status determines germ cell meiotic commitment in embryonic and postnatal mammalian gonads. Cell Cycle *9*, 339–349.

Watanabe, T., Takeda, A., Tsukiyama, T., Mise, K., Okuno, T., Sasaki, H., Minami, N., and Imai, H. (2006). Identification and characterization of two novel classes of small RNAs in the mouse germline: retrotransposon-derived siRNAs in oocytes and germline small RNAs in testes. Genes Dev. *20*, 1732–1743.

Weiss, R.S., Matsuoka, S., Elledge, S.J., and Leder, P. (2002). Hus1 acts upstream of chk1 in a mammalian DNA damage response pathway. Curr. Biol. *12*, 73–77.

Yabuta, Y., Kurimoto, K., Ohinata, Y., Seki, Y., and Saitou, M. (2006). Gene expression dynamics during germline specification in mice identified by quantitative single-cell gene expression profiling. Biol. Reprod. *75*, 705–716.

Yang, F., Eckardt, S., Leu, N.A., McLaughlin, K.J., and Wang, P.J. (2008). Mouse TEX15 is essential for DNA double-strand break repair and chromosomal synapsis during male meiosis. J. Cell Biol. *180*, 673–679.